



Reconciling Discrepancies between Uk37 and Mg/Ca Reconstructions of Holocene Marine Temperature Variability

Citation

Laepple, Thomas R., and Peter John Huybers. 2013. "Reconciling Discrepancies between Uk37 and Mg/Ca Reconstructions of Holocene Marine Temperature Variability." *Earth and Planetary Science Letters* 375 (August): 418–429.

Published Version

doi:10.1016/j.epsl.2013.06.006

Permanent link

<http://nrs.harvard.edu/urn-3:HUL.InstRepos:13454549>

Terms of Use

This article was downloaded from Harvard University's DASH repository, and is made available under the terms and conditions applicable to Open Access Policy Articles, as set forth at <http://nrs.harvard.edu/urn-3:HUL.InstRepos:dash.current.terms-of-use#OAP>

Share Your Story

The Harvard community has made this article openly available.
Please share how this access benefits you. [Submit a story](#).

[Accessibility](#)

Reconciling discrepancies between Uk37 and Mg/Ca reconstructions of Holocene marine temperature variability

Thomas Laepple¹ and Peter Huybers²

¹Alfred Wegener Institute for Polar and Marine Research
Bremerhaven, Germany

²Department of Earth and Planetary Sciences, Harvard University
Cambridge, USA

Abstract

Significant discrepancies exist between the detrended variability of late-Holocene marine temperatures inferred from Mg/Ca and Uk37 proxies, with the former showing substantially more centennial-scale variation than the latter. Discrepancies exceed that attributable to differences in location and persist across various calibrations, indicating that they are intrinsic to the proxy measurement. We demonstrate that these discrepancies can be reconciled using a statistical model that accounts for the effects of bioturbation, sampling and measurement noise, and aliasing of seasonal variability. The smaller number of individual samples incorporated into Mg/Ca measurements relative to Uk37 measurements leads to greater aliasing and generally accounts for the differences in the magnitude and distribution of variability. An inverse application of the statistical model is also developed and applied in order to estimate the spectrum of marine temperature variability after correcting for proxy distortions. The correction method is tested on surrogate data and

shown to reliably estimate the spectrum of temperature variance when using high-resolution records. Applying this inverse method to the actual Mg/Ca and Uk37 data results in estimates of the spectrum of temperature variance that are consistent. This approach provides a basis by which to accurately estimate the distribution of intrinsic marine temperature variability from marine proxy records.

Keywords: Holocene climate variability, signal and noise in proxies, multiproxy comparison, spectral analysis, SST variability

1. Introduction

Although Mg/Ca and Uk37 proxies are used to infer the same physical attribute of near-surface marine temperature, the recorded temperature signals reflect disparate life cycles and biophysical functioning of the proxy producing organisms and disparate incorporation and preservation of the signal in sediments. Potential contributions include non-temperature influences on the incorporation of Mg/Ca into foraminiferal shells (Arbuszewski et al., 2010), re-suspension and redeposition of Uk37 markers (Ohkouchi et al., 2002), and other possible post-depositional effects on Mg/Ca (Regenberg et al., 2006) and Uk37 (Hoefs et al., 1998; Gong and Hollander, 1999). These considerations make it important to infer temperatures from multiple sources and evaluate their consistency (e.g. De Vernal et al., 2006).

Previous studies noted that the temperature variability inferred for the last millenium differ according to the proxy type used (Richey et al., 2011). Proxy dependence has also been noted for the temporal patterns of deglacial warming (Steinke et al., 2008; Mix, 2006) and mid- to late-Holocene tem-

17 perature trends (Leduc et al., 2010; Lohmann et al., 2012). Differences be-
18 tween Mg/Ca and Uk37 derived temperatures have been suggested to arise
19 from differences in seasonal recording (Leduc et al., 2010; Schneider et al.,
20 2010). How orbital variations manifest in proxy records sensitively depends
21 on how the seasonal cycle is recorded (e.g., Huybers and Wunsch, 2003;
22 Laepple et al., 2011), and this effect might explain diverging multi-millennial
23 signals between proxies, or at least some fraction of the differences over the
24 Holocene (Lohmann et al., 2012). Importantly, however, the ten-thousand-
25 year timescale orbital variations are not expected to explain the differences in
26 millennial and higher-frequency variability that are focused on in this study.

27 Here, we explore the discrepancies between Mg/Ca and Uk37 proxies
28 of sea surface temperature at centennial to millennial timescales, identify a
29 physical-statistical model for their origin, and present a method to correct
30 for the associated biases when estimating temperature variance. Although it
31 would be possible to interpret each individual proxy—or record or even single
32 sample—as a unique perspective on past temperature, the emphasis here is
33 to statistically account for distinctions between proxy measurements for the
34 purposes of facilitating synthesis between records and comparison with in-
35 strumental observations and model simulations of temperature. In contrast
36 to typical synthesis efforts that focus on reconstructing the time-history of
37 temperature, we seek to estimate the magnitude of temperature variability as
38 a function of timescale or, more precisely, the spectral distribution of sea sur-
39 face temperature variability at centennial to millennial frequencies. Beyond
40 holding intrinsic interest, quantitative estimates of temperature variability
41 prior to the anthropogenic era and at frequencies lower than those afforded

by instrumental records are generally needed when seeking to interpret specific changes in temperature and attribute them to a set of causes (e.g., Barnett et al., 1999).

2. Data and Methods

We focus our analysis on the two most prominent proxies of near-surface marine temperature, Mg/Ca ratios from planktic foraminifera (Lea et al., 1999) and the Uk37 ratio of different long-chain ketones (Brassell et al., 1986). Both proxies are recovered from sediment cores and are affected by bioturbation. An important distinction, however, is that each Mg/Ca measurement is typically made using a small number of crushed planktic foraminifera, usually about 30, whereas Uk37 is an organic proxy that is sampled from millions of molecules.

2.1. Proxy and instrumental data

The proxy dataset assembled for this study aims to be comprehensive in the sense of including all sufficiently long and well-resolved sediment records that cover the mid- to late-Holocene. Most Mg/Ca and Uk37 records are from the GHOST database (Leduc et al., 2010), though also included are two recently published high-resolution Mg/Ca records: MV99-GC41/PC14 (Marchitto et al., 2010) and MD99-2203 (Cleroux et al., 2012). Specifically, we include 6 planktonic Mg/Ca records from *G.ruber* and *G.bulloides* and 16 Uk37 records, all of which are dated by radiocarbon and have an average sampling rate of 100 years or less (Figure 1). Lower resolution records are excluded in the analysis because it is then difficult to accurately correct for sampling effects, as is later demonstrated.

66 All proxy records of a given type are recalibrated in a uniform manner to
 67 facilitate intercomparison. Uk'37 records are calibrated using $0.033 \text{ Uk37}/^\circ\text{C}$,
 68 Uk37 records using $0.035 \text{ Uk37}/^\circ\text{C}$, and Mg/Ca records using $9.35\% \text{ Mg/Ca}$
 69 per $^\circ\text{C}$. These choices are the mean of all author calibrations of the analysed
 70 datasets but also agree with the standard calibrations given by Mueller et al.
 71 (1998) ($0.033 \text{ Uk'37}/^\circ\text{C}$) and Dekens et al. (2001) ($9\% \text{ Mg/Ca per } ^\circ\text{C}$).
 72 See Table 1 and Figure 1 for more details regarding individual records. In-
 73 strumental observations that we later use to model the proxy recording pro-
 74 cess are from the HADSST3 compilation of sea surface temperatures (SST)
 75 (Kennedy et al., 2011b,a).

76 *2.2. Spectral estimation*

77 Spectral estimates are used to quantify timescale dependent variability.
 78 Although techniques exist to estimate spectra from unevenly sampled data
 79 (Lomb, 1976), our experimentation with synthetic signals indicates that more
 80 accurate results are obtained by first interpolating to a uniform sampling rate
 81 and then employing state-of-the-art spectral estimation techniques. Linear
 82 interpolation of an unevenly sampled record tends both to reduce the energy
 83 at the highest frequencies of a spectral estimate and to alias variability into
 84 lower frequencies (Rhines and Huybers, 2011).

85 To minimize the influence of high-frequency damping, we determine the
 86 finest interpolation resolution for which the frequency spectrum is largely
 87 unbiased. For an evenly sampled record, the optimal interpolation resolu-
 88 tion would equal the sampling resolution, but for unequal time steps the
 89 optimal interpolation resolution is no longer obvious, and we employ a nu-
 90 merical method to determine an appropriate value. This process involves

91 generating random numbers that follow a power-law processes with $\beta = 1$;
 92 subsampling these synthetic time series according to the sampling sequence
 93 of a given proxy record, and then interpolating to a resolution equal to the
 94 finest sampling time step of the original record. The spectral estimate of the
 95 resampled stochastic process is divided by the theoretical spectra, and the
 96 highest reliable frequency is determined by when this ratio crosses a value
 97 of 0.7. The selected interpolation resolution is then set to resolve the identi-
 98 fied frequency, with the selected value rounded to the nearest 50 years and
 99 referred to as the optimal interpolation resolution. The optimal interpola-
 100 tion resolution depends on the evenness of the sampling. For example, core
 101 D13882 has a 53 year mean sampling resolution but contains some 140 year
 102 gaps, and the optimal interpolation resolution is 200 years, whereas other
 103 cores with a similar mean sampling rate have a 100 year optimal resolution.

104 To minimize issues associated with aliasing, data are first linearly inter-
 105 polated to ten times the optimal resolution, lowpass filtered using a finite
 106 response filter with a cut-off frequency of 1.2 divided by the target time step,
 107 and then resampled at the optimal resolution.

108 Spectra are estimated using Thomson’s multitaper method (Percival and
 109 Walden, 1993) with three windows. Time series are detrended prior to anal-
 110 ysis, as is standard for spectral estimation. The multitaper approach in-
 111 troduces a small bias at the lowest frequencies and we omit the two lowest
 112 frequencies in all figures. For visual display purposes, power spectral esti-
 113 mates are also smoothed using a Gaussian kernel with constant width in
 114 logarithmic frequency space (Kirchner, 2005), when using logarithmic axes.
 115 When the smoothing kernel extends outside of the frequency range resolved

116 by a record, it is truncated at both the low- and high-frequency ends of the
117 kernel to maintain its symmetry and to avoid biasing estimates.

118 Our focus will be on the average power spectral estimate for each proxy
119 type because this gives an improved signal-to-noise ratio and facilitates inter-
120 comparison between proxy types. This average power spectrum for each
121 proxy type necessarily contains samples from regions with differing variabil-
122 ity and that cover different frequency intervals. To avoid discontinuities
123 across frequencies where the number of available estimates change, proxy
124 spectra are scaled to an average value in the largest common frequency in-
125 terval. Note that it is the spectral estimates that are averaged together,
126 giving an estimate of the spectral energy, and that this is distinct from av-
127 eraging together records in the time-domain, which would give an estimate
128 of mean temperature.

129 Records are not intercompared in the time domain because timing errors
130 generally destroy covariance and coherence. Spectral estimates, however,
131 are largely insensitive to timing errors when the underlying process follows
132 a power-law (Rhines and Huybers, 2011), which appears a good approx-
133 imation for the proxy records considered here. Thus, intercomparison of
134 spectral estimates derived from proxy records with uncertain timing is feasi-
135 ble. Power laws are estimated by a least-squares fit to logarithmic frequency
136 and logarithmic power-density estimates (Huybers and Curry, 2006). To
137 more uniformly weight the estimate, spectra are binned into equally spaced
138 log-frequency intervals and averaged before fitting. Power-laws are only
139 estimated in a frequency range common to all proxy records, $1/2000\text{yr}$ to
140 $1/400\text{yr}$.

141 3. Discrepancies between Mg/Ca and Uk37

142 On average, the Mg/Ca reconstructions of temperature have 2.2 times
143 greater variance than Uk37 reconstructions, when making comparisons at
144 150 year resolution. This discrepancy in variance is visually apparent (Figure
145 1). There are several possibilities for the differences in variance. One is that
146 the actual temperature variability at the Mg/Ca sites is greater than that
147 at the Uk37 sites. Instrumental records from HadSST3 show the opposite,
148 however, that Uk37 sites have between 1.2-1.5 times more variance than the
149 Mg/Ca sites, depending on the season that is considered. Furthermore, a
150 latitudinal comparison shows that Mg/Ca is the more variable within given
151 regions (Figure 2), and similar results hold when sectors are defined according
152 to longitude and latitude.

153 Another possibility has to do with differences or uncertainties in the cal-
154 ibration of proxies to temperature. Choosing the most sensitive calibration
155 for Mg/Ca ($0.107 \text{ (Mg/Ca)/}^\circ\text{C}$ (Mashiotto et al., 1999)) and the least sen-
156 sitive calibration for Uk37 ($0.023 \text{ Uk37/}^\circ\text{C}$, (Sonzogni et al., 1997)) gives an
157 average variance that is similar for the two proxy types, but applying such
158 calibrations globally is almost certainly inappropriate. The low sensitivity
159 Uk37 calibration was developed for a region near the upper temperature limit
160 of this proxy ($24\text{-}29^\circ\text{C}$), and Sonzogni et al. (1997) actually suggest a global
161 temperature calibration for Uk37 ($0.031 \text{ Uk37/}^\circ\text{C}$) similar to the mean cali-
162 bration used in this study. Moreover, rescaling the variability employing any
163 single calibration would not resolve discrepancies in the relative distribution
164 of fast and slow variability, which is discussed in more detail later.

165 A final consideration is whether the proxies record different seasons and,

166 therefore, show systematically different amounts of variability. Such a mecha-
 167 nism would work for monthly to interannual time-scales where, for example,
 168 extratropical winter sea surface temperatures are generally more variable
 169 than summer or annual mean temperatures because of greater storm activity
 170 (Wallace et al., 1990). Analysis of a state-of-the-art coupled climate model,
 171 MPI-ESM (Jungclauss et al., 2010), shows this seasonal distinction in vari-
 172 ability at short timescales, but that the distinction in variability is no longer
 173 identifiable at the positions of the Mg/Ca and Uk37 records at frequencies
 174 below 1/100 years. These model results indicate that seasonal differences
 175 in when temperatures are recorded to be an inadequate explanation of the
 176 discrepancy.

177 A more detailed picture of the discrepancy in variability between the two
 178 proxies can be obtained through spectral analysis. The spectra of each proxy
 179 record in the compilation is estimated using a multitaper procedure. Though
 180 consistent results are found evaluating single records, these comparisons are
 181 noisy, and we instead focus on the average spectra across each proxy type
 182 (Figure 2). Both the Mg/Ca and Uk37 spectral averages show increased en-
 183 ergy toward lower frequencies, but the magnitude and detailed shape of these
 184 estimates are incommensurate in that Mg/Ca records have proportionately
 185 more high- than low-frequency variability than Uk37. The energy found at
 186 millennial (1-3kyr) relative to centennial variability (200yr-500yr) is 3.6 for
 187 Uk37 and 2.0 for Mg/Ca, a relative difference that is unaffected by calibration
 188 choice.

189 More generally, the spectra can be described using a powerlaw scaling,
 190 $f^{-\beta}$, where f is frequency in cycle per year and β is the power-law exponent.

191 Spectral energy increases less steeply with decreasing frequency in Mg/Ca,
192 which has $\beta_{Mg/Ca} = 0.58$, than in Uk37, which has $\beta_{Uk37} = 0.98$.

193 The discrepancies between Uk37 and Mg/Ca variance and distributions of
194 spectral energy generally exceed a factor of two, and it appears necessary to
195 resolve these discrepancies prior to being able to infer temperature variability
196 to within this factor. An accurate estimate of the temperature spectrum is
197 important because it would directly indicate the range of natural temperature
198 variation expected over a given timescale, indicate the physics that controls
199 temperature variations, and serve as the basis for a test of whether climate
200 models adequately represent climate variability (Hasselmann, 1976; Barnett
201 et al., 1996; Pelletier, 1998; Huybers and Curry, 2006).

202 4. Proxy correction technique

203 We posit that the difference in variability between proxy types arises from
204 processes that can be grouped into three categories: (1.) errors in tempera-
205 ture estimates arising from measurement noise, vital effects, and changes in
206 depth habitats (Schiffelbein and Hills, 1984), (2.) irregular and/or infrequent
207 sampling times that cause aliasing of seasonal and other high-frequency vari-
208 ability (Kirchner, 2005; Laepple et al., 2011), and (3.) bioturbation that
209 mixes samples across time horizons (Berger and Heath, 1968). A number
210 of other sources of uncertainty are also present but we assume and later
211 confirm that they do not have first-order implications for the recorded vari-
212 ability. Building on existing models for these noise sources, we attempt to
213 quantify their aggregate influence upon the spectra of each proxy using a
214 single statistical model. We will also show that such a representation can

215 be inverted to better estimate the frequency spectrum of temperature from
 216 proxy records.

217 4.1. Basics of the approach

218 Any given temperature record that we consider, y , has a spectral esti-
 219 mate, $S_{\hat{y}}$, that is corrupted by noise. Here we seek a best estimate of the
 220 true power spectrum, $S_{\hat{x}}$, using a correction that relies upon the biophysical
 221 characteristics of the proxy sampling process. For this correction we apply
 222 the spectral filtering approach of Kirchner et al. (2005) wherein a statis-
 223 tical model is constructed of the sampling process—including bioturbation,
 224 measurement, and other intrasample noise—and a filter is designed from the
 225 output of the model for the purposes of optimally estimating the true power
 226 spectrum.

227 Given a perfect model of the true spectrum, S_{xm} , and the sampled spec-
 228 trum, S_{ym} , an optimal estimate of the true temperature spectrum, $S_{\hat{x}}$, can
 229 be obtained,

$$S_{\hat{x}} = S_{\hat{y}} \frac{S_{xm}}{S_{ym}}, \quad (1)$$

230 where the fractional term involving the model spectra is equivalent to a
 231 filter. We use a piecewise model of the true temperature spectrum that calls
 232 on observed instrumental temperature at high frequencies and a power-law
 233 at low frequencies, as has been found adequate for describing the spectral
 234 scaling of many other proxy records (Huybers and Curry, 2006),

$$S_{xm} = \begin{cases} cf^{-\beta}, & f \leq f_c \\ S_{\hat{x}i}, & f_c > f \end{cases}. \quad (2)$$

235 The frequency range extends from the lowest frequency sampled by the ob-
 236 served record to once per two years. Higher frequency variability is separately

237 treated in the sampling process. $S_{\hat{x}i}$ is the spectral estimate from the ob-
 238 served SST and c is chosen to ensure that both pieces of the spectra meet
 239 at the cutoff frequency, f_c . The cutoff frequency is set at 1/50yr, the lowest
 240 frequency constrained by the instrumental record. The power-law, β , is an
 241 adjustable parameter constrained to take on values between zero and two. A
 242 value of β equal to zero corresponds to white noise, whereas values in excess
 243 of one, but not greater than two, have previously been found in proxy records
 244 that span glacial-interglacial variability (Huybers and Curry, 2006).

245 4.2. Bioturbation and sampling

246 Bioturbation is represented assuming a well-mixed sediment layer whose
 247 thickness is taken as an adjustable parameter (Berger and Heath, 1968). This
 248 gives an impulse response function, g , that fully describes the mixing response
 249 over the thickness of the bioturbation layer, δ (Guinasso and Schink, 1975).
 250 A $\delta = 10\text{cm}$ bioturbational layer is typical of marine sediments (Boudreau,
 251 1998; Guinasso and Schink, 1975) and is our default parameter, but we also
 252 examine the robustness of our results using 2 and 20cm layers. Because
 253 sediment cores have different mean accumulation rates, a , the timescale as-
 254 sociated with bioturbational smoothing varies. No bioturbation is imposed
 255 for cores MV99-GC41/PC14 (Marchitto et al., 2010) and SO90-39KG/56KA
 256 (Dooze-Rolinski et al., 2001) because they are laminated.

257 Uk37 samples comprise very large numbers of organic molecules, and we
 258 approximate such sample as continuous. The sampling can be described as
 259 a convolution of the temperature time series with the bioturbation impulse
 260 response function in the time domain, but for the purposes of describing the
 261 influence at a particular time horizon we cast the response as a sum across

262 annual time steps,

$$y(t_i) = \sum_j x(t_{i+j})g(j) + \eta(t_i). \quad (3)$$

263 Although the sum is nominally over the entire depth of the core, in practice,
264 we sum from $3\delta/a$ above to $1\delta/a$ below the time horizon of interest. This
265 time interval of four times the bioturbational layer divided by the accumu-
266 lation rate contains 99% of the weight in the impulse response, g . The noise
267 component, $\eta(t_i)$, represents the measurement error as well as other intra-
268 test variations, such as those caused by variations in depth habitat, and is
269 assumed independent between samples and normally distributed.

270 Mg/Ca samples comprise a discrete sample of foraminifera tests, usu-
271 ally ranging between values of 20 to 60 for planktic samples. The sampling
272 process is divided into interannual and subannual components for purposes
273 of computational efficiency. The interannual component is selected as the
274 annual average temperature, $x(t + \epsilon)$, where ϵ represents timing offsets intro-
275 duced by bioturbation and is randomly selected according to the probability
276 distribution defined by g . An additional noise term is then added to represent
277 subannual variability, giving $x(t + \epsilon) + \psi(m)$. The value of $\psi(m)$ is selected
278 as the monthly temperature anomaly from the climatological seasonal cycle,
279 where the month is randomly chosen according to the modern lifecycle of
280 the specific foraminiferal species at that core site simulated by a dynamic
281 population model, PLAFOM (Fraile et al., 2008),

$$y(t_i) = \frac{1}{N} \sum_{j=1}^N [x(t_i + \epsilon_j) + \psi(m_j)] + \eta(t_i). \quad (4)$$

282 Thus, as opposed to the case of Uk37 samples, the sum is across each of the
283 N foraminifera comprising a sample.

284 4.3. Detailed example

285 The foregoing technique is described in detail with respect to a single
286 Mg/Ca record in order to provide greater insight into the implications of
287 the sampling and bioturbation model. We focus on a Mg/Ca record from
288 *G. ruber* tests in core MD03-2707 (Weldeab et al., 2007) as being broadly
289 representative of our approach and discuss how this analysis compares with
290 that of Uk37 records. MD03-2707 was taken from the Gulf of Guinea, is
291 associated with a mean sedimentation rate of 55cm/kyr, and is sampled at
292 a mean resolution of 37 years. The PLAFOM model (Fraile et al., 2008)
293 indicates a seasonality in *G. ruber* population in the Gulf of Guinea that
294 peaks between June and October. SSTs exhibit an annual cycle of 3.4°C
295 amplitude at this location (Rayner et al., 2006) and are coolest between
296 June and October. Therefore, the uneven sampling of these SSTs leads to a
297 bias toward cooler temperatures (Fig. 3a,b).

298 Importantly, the sampling of the seasonal cycle in SST by foraminiferal
299 tests contains a significant stochastic component, depending on the individ-
300 ual lifecycle of the approximately 30 samples that are crushed and collected
301 together for each Mg/Ca measurement. This random component of how the
302 seasonal cycle is sampled gives, in this case, a standard deviation between
303 samples of 0.24°C (Fig. 3c,d). Although the number of Mg/Ca tests averaged
304 together would be sufficient to resolve the seasonal variability, the nonuni-
305 form distribution leads to a stochastic aliasing of the seasonal variability.

306 The magnitude of aliased noise is different for every core, depending on
307 the seasonality of SST and foraminifera populations as well as the number
308 of tests averaged together for each Mg/Ca sample, thus necessitating that

we model this process independently for each record. A positive correlation ($R=0.49$, $p>0.1$) between the variance of the Mg/Ca records and the modern seasonal range of SST at the position of the cores (Table 1) indicates the importance of this process. Note that there is one outlier among the Mg/Ca samples from core MD99-2203 (Cleroux et al., 2012) whose omission would raise the cross-correlation to $R=0.85$. In contrast, the Uk37 variance is not expected to show such seasonal aliasing and is uncorrelated to the seasonal range. An interesting feature of this effect is that inasmuch as Mg/Ca samples are evenly distributed over the year—a feature usually considered to be advantageous—greater aliasing generally occurs because the finite number of samples are distributed over a larger range of seasonal variability.

Bioturbation is the other process in our model that significantly influences recorded variability. For Mg/Ca the influence of bioturbation is a random process that depends on what portions of the seasonal cycle happen to be sampled. To illustrate the effects of bioturbation, we generate synthetic proxy records consistent with the characteristics of the Gulf of Guinea site MD03-2707 following the piecewise spectral representation given in Eq. 2. To generate a record whose variability is consistent with that observed in instrumental SSTs nearest the core site, the Fourier transform of white noise is multiplied by the instrumental SST spectra and then transformed back into a time series. Lower frequency variability that is not covered by the instrumental records are initially parameterized to follow a power-law of $\beta = 1$ (Fig. 4). The correct value of β is uncertain and a search is made over a range of plausible values.

Bioturbation is assumed to extend down $\delta = 10\text{cm}$ into the sediment,

334 which equates to 182 years in this core, given the average accumulation rate.
 335 In the case of Uk37, where the number of samples are essentially infinite,
 336 bioturbation leads to a smoothed and time lagged version of the SST record.
 337 But in the case of Mg/Ca the discrete sampling discussed in the foregoing
 338 paragraph adds variability that the bioturbation only partially reduces. For
 339 core MD03-2707 we find that aliasing contributes more variance than biotur-
 340 bation suppresses, such that the resulting Mg/Ca record is expected to have
 341 more variability than the actual SST record. This increase in temperature
 342 variance inferred from Mg/Ca records is found to generally hold across the
 343 records in our collection.

344 Finally, measurement noise and other sources of intratest variability are
 345 represented by addition of white noise, η . The noise standard deviation
 346 must be estimated from the proxy record, along with the value β , and in
 347 the case of MD03-2707 has a standard deviation of 0.5°C . The results of
 348 aliasing, bioturbation, and measurement noise are illustrated in Fig. 5 where
 349 a synthetic time series is sampled in accord with that of Uk37 and Mg/Ca
 350 samples. The resulting smoothing and aliasing are clearly evident. Note
 351 that increasing the number of individual foraminifera in a Mg/Ca sample,
 352 N , leads to a more stable value of $\frac{1}{N} \sum \psi(m_j)$ and results that are more
 353 consistent with that of Uk37. For $N = \infty$, the Mg/Ca and Uk37 results
 354 are identical in our models, excepting a possible mean offset associated with
 355 disproportionate sampling of the climatological seasonal cycle.

356 5. Application of the correction filter

357 Determining the most suitable correction filter (Eq. 1) for each record
358 requires estimating the two adjustable parameters that define the background
359 variability: the spectral slope β and the standard deviation associated with η .
360 We perform an exhaustive search over the values of $\beta = \{0, 0.1, \dots 1.9, 2.0\}$ and
361 $\text{STD}(\eta) = \{0, 0.05, \dots 1.95, 2\}$, searching for the pair of values that minimize
362 the mean square deviation between the logarithm of the observed spectra
363 and the logarithm of the model spectra.

364 Sea surface temperature time series are generated in accord with each
365 combination of the adjustable parameters, after which the bioturbation and
366 sampling models are applied to produce a synthetic proxy record. This pro-
367 cess is repeated 1000 times to approximate the distribution of possible results,
368 with the spectra of the uncorrupted and corrupted version of the synthetic
369 time series being recorded in each instance. Prior to performing the spectral
370 analysis, records are interpolated to a uniform spacing in direct correspon-
371 dence with the actual proxy record being represented. The average spectral
372 estimate associated with the uncorrupted time series, $S_{\hat{x}m}$, is then divided
373 by the average spectral estimates of the corrupted time series, $S_{\hat{y}m}$, to yield
374 a filter. Following Eq. 1, multiplication of each filter times the correspond-
375 ing spectral estimate associated with a given proxy record yields our best
376 estimate of the spectrum of SST variability at that site.

377 *5.1. Test of the filtering approach on synthetic data and estimation of confi-*
 378 *dence intervals*

379 Before applying the proxy correction technique described above to the
 380 data, we first test its performance on surrogate time series. Surrogate time
 381 series are generated in accord with Eq. 2. High frequency variability is real-
 382 ized to be consistent with that observed in instrumental SSTs nearest each
 383 site, whereas lower frequencies follow a power-law of $\beta = 1$. For both Uk37
 384 and Mg/Ca, the sample spacing from each core is applied, a 10cm biotur-
 385 bation depth is assumed, and a 0.25 and 0.45 standard deviation of η is
 386 prescribed for Uk37 and Mg/Ca respectively. Additional parameters are also
 387 prescribed for each Mg/Ca record comprising the population seasonality from
 388 PLAFOM, instrumental SST seasonality, and the reported number of foram-
 389 inifera tests in each sample (see Fig. 6). To test the effect of the sampling
 390 resolution on our method we also include two lower resolution cores in this
 391 analysis (MD01-2378 (Xu et al., 2008) and MD95-2043 (Cacho et al., 2001))
 392 which are not used in the remaining part of the study.

393 The correction algorithm yields more accurate results given more highly
 394 resolved records. In particular, β is only well constrained when the sampling
 395 interval averages less than 100 years, especially for Mg/Ca records where
 396 aliasing of the seasonally cycle is of particular concern. Synthetic records
 397 with a larger average sampling interval also show biases in their associated
 398 estimates, and we therefore restrict the data used in this study to records
 399 with a mean sampling resolution of less than 100 years. We also find that
 400 power-law estimates begin to show bias for processes having a true power-
 401 law less than 0.1 for Uk37 and less than 0.7 for Mg/Ca records (Fig. 7). As

we will show later, application of the spectral correction algorithm to the Holocene proxy records gives values of β near one. Therefore, the synthetic experiments indicate that the application of the spectral correction algorithm will yield accurate results when applied to the data in our collection.

We also use this surrogate approach to estimate the uncertainties associated with spectral estimation and the filtering process. Specifically, we simulate surrogate time series using the estimated β scaling relationship, then corrupt the records according to the properties associated with each actual record, apply the correction algorithm, and estimate the resulting average spectra. This algorithm is repeated one-thousand times, and a chi-square distribution is fit to the ensemble of results at each frequency using moment matching. The reported uncertainty estimates thus include the effects of the proxy correction technique along with the usual uncertainties associated with making a spectral estimate of a noisy and finite process.

5.2. Application to the actual data

Application of the correction filter to the individual Uk37 records leads to a 35% overall reduction in variance or, equivalently, spectral energy (Fig. 8a). The initial power-law associated with the average spectra of 0.98 only changes to 0.96 after correction, indicating that the overall shape of the spectra is only slightly altered. Application of the correction filter to the Mg/Ca records results in a 60% reduction in variance (Figure 8b). This large decrease in energy in the corrected estimates can be traced to the relatively small number of individual foraminifera combined together for each Mg/Ca estimate and the resulting aliasing and intrasample variability. Furthermore, the strongest relative reduction of variance occurs at the highest frequencies, causing β to

427 change from 0.58 to 1.05 for the average Mg/Ca spectral estimate.

428 Upon applying our correction algorithm, the Uk37 and Mg/Ca power-law
429 scaling coefficients become consistent with one another to within uncertainty,
430 with values of $\beta_{Uk37} = 0.96 \pm 0.07$ and $\beta_{Mg/Ca} = 1.05 \pm 0.07$ (Figure 8c).
431 The variance of Mg/Ca is decreased by the correction algorithm so that, on
432 average, these records are only 20% more variable than the Uk37 records, a
433 discrepancy that is well within the uncertainty in the calibrations for Mg/Ca
434 and Uk37. Note that calibration uncertainty does not influence the power-
435 law estimates, making the Uk37 and Mg/Ca power-law consistency the more
436 stringent indicator of the correction algorithm's adequacy.

437 Independent information from the reported measurement and replicate
438 measurements of Mg/Ca can also be used to evaluate the correction method.
439 The correction filter has two parameters: β which describes the scaling be-
440 havior of the underlying temperature signal and η which describes the stan-
441 dard deviation of the random variations introduced by measurement error
442 and all other processes except those associated with sampling and bioturba-
443 tion. Values of β and η are determined from a two-dimensional parameter
444 search for minimum misfit between the modeled and observed spectral esti-
445 mate, and the contours representing this misfit (Fig. 9a-b) indicate that the
446 standard deviation of η is constrained near 0.25°C and 0.5°C for Uk37 and
447 Mg/Ca, respectively. The mean reported replicate error for Uk37 measure-
448 ments is 0.23°C, corresponding in magnitude to the estimates made here.
449 A close relationship also exists between the inferred and reported errors for
450 Mg/Ca records across the four records for which replicate results are available
451 (Figure 9c). The fact that the correction algorithm gives results that inde-

pendently agree with the reported replicate error statistics further indicates that it yields accurate results.

6. Summary and conclusion

The differing temperature variability indicated by Uk37 and Mg/Ca records can be reconciled through correcting for the effects of aliasing, bioturbation, and other noise sources. The correction brings the overall variance or, equivalently, the average spectral energy between the Uk37 and Mg/Ca record into greater agreement, reducing the 100% greater Mg/Ca variance to having only 20% more variance. The residual difference can be accounted for by uncertainties in the temperature calibrations applied to either or both of the proxy types. The correction also brings the power-law scaling associated with each proxy into consistency within relatively small uncertainties.

Mg/Ca temperature estimates are strongly affected by aliasing of seasonal and interannual temperature variability due to the limited number of foraminiferal tests used in a given measurement, with additional variability contributed by measurement error, intra-sample variations (e.g. Sadekov et al., 2008), and issues associated with the cleaning processes (Barker, 2003). In contrast, Uk37 temperature estimates comprise a large number of molecules and do not admit seasonal and interannual aliasing. Accordingly, the estimated noise term for Uk37 measurements is about half that of the Mg/Ca proxy. Bioturbation is of secondary importance in this collection of records because they all are associated with high-accumulation rates.

Holocene sea surface temperature variability is found to follow a power-law scaling close to one at timescales between century and millennia. Earlier

476 marine proxy studies found larger-magnitude scaling coefficients (Pelletier,
477 1998; Shackleton and Imbrie, 1990; Huybers and Curry, 2006), though this is
478 not surprising because they examined variability over glacial-interglacial time
479 scales. Glacial climates and the transition from glacial to inter-glacial cli-
480 mates show different frequency scaling behavior than the Holocene interval
481 (Ditlevsen et al., 1996). We also note that previous studies made no cor-
482 rections to their spectral estimates, and that such correction could increase
483 the discrepancy insomuch as aliasing contributes energy at high frequen-
484 cies, but might also increase consistency because bioturbation is expected to
485 have a larger influence on records associated with lower accumulation rates.
486 Regardless, the effect of those corrections on the spectral scaling of glacial-
487 interglacial temperature evolution would likely be smaller than found in our
488 analysis of Holocene record because of much larger amplitude temperature
489 variability and, presumably, a higher signal-to-noise ratio. It will be of in-
490 terest in future studies to examine how climate spectra vary as a function of
491 background climate, and such an analysis is now more feasible because the
492 present method should, at least in principle, also permit for correcting for
493 artifacts associated with changes in signal-to-noise ratios.

494 Although seasonal differences in the abundance of proxy indicators are
495 usually regarded as a disadvantage in climate reconstructions because it bi-
496 ases the estimate away from the annual mean (Wunsch, 2009; Laepple et al.,
497 2011), it can be an advantage when one aims to reconstruct the amplitude
498 of climate variability. A site with an equal foraminiferal flux over the year,
499 especially at a site with strong seasonality in temperature, is more prone to
500 aliasing of the seasonal cycle into the recorded signal as the small amount of

501 samples are distributed over the whole range on the seasonal cycle. A further
502 concern does arise, however, that the seasonal distribution of the foramin-
503 fera flux is most likely a function of the background climate itself and such
504 nonstationarities have not been accounted for in the present analysis.

505 There are a number of other processes that might also corrupt proxy
506 records. Uk37 markers might be affected by advection and redistribution
507 (Ohkouchi et al., 2002) or preferential degradation of either one of the long
508 chain alkenones (Hoefs et al., 1998; Gong and Hollander, 1999) or the Mg/Ca
509 rich calcite in foraminifera (Regenberg et al., 2006). At least for degrada-
510 tion influences, we expect that these will mainly act on the trends and not
511 strongly distort the continuum spectra of variability. As noted earlier, all
512 records analyzed here have been detrended prior to making spectral esti-
513 mates. Given that there is no expectation for the above mentioned sources
514 of error to affect Mg/Ca and Uk37 records equally, the result that both Uk37
515 and Mg/Ca records show a similar spectrum of variability after correction
516 suggests that the major sources of corruption in the temperature signal have
517 been accounted for. Agreement between the estimated and observed repli-
518 cate noise values further indicates that no major contributions to error have
519 been overlooked.

520 These results also highlight the utility of smoothing Mg/Ca records, as
521 is often all ready done in practice (e.g. Marchitto et al., 2010). The recon-
522 structed temperature spectra show strong autocorrelation whereas the noise
523 component is close to being uncorrelated. Therefore, smoothing is expected
524 to more completely suppress noise variance relative to that of the tempera-
525 ture signal and, thereby, to increase the signal-to-noise ratio. It should be

possible to design a filter that would optimally increase signal-to-noise ratios in a given Mg/Ca time series or other proxy records. We conclude that the correction algorithm presented here provides a basis by which to more accurately estimate marine temperature variance and its spectral distribution and should provide further insight into how to optimally control for noise sources.

Acknowledgments

We thank Tom Marchitto, Peter DeMenocal, Caroline Cleroux, Peter Stott, and Elizabeth Farmer for information regarding replicates; Jung-Hyun Kim and Guillaume Leduc for providing the GHOST dataset, Igaratza Fraile for providing the PLAFOM results and Stephen Barker, Gerrit Lohmann, Cristian Proistosescu, Andy Rhines, Stephan Dietrich, and Alexander Stine for helpful discussion. We also thank Julian Sachs and an anonymous reviewer for their constructive comments. TL was supported by the Alexander von Humboldt foundation and the Daimler and Benz foundation and PH received support from NSF award 0960787.

References

- Arbuszewski, J., deMenocal, P., Kaplan, A., Farmer, E. C., Dec. 2010. On the fidelity of shell-derived ^{18}O seawater estimates. *Earth and Planetary Science Letters* 300 (3-4), 185–196.
- Barker, S., 2003. A study of cleaning procedures used for foraminiferal Mg/Ca paleothermometry. *Geochemistry Geophysics Geosystems* 4 (9).

548 Barnett, T., Hasselmann, K., Chelliah, M., Delworth, T., Hegerl, G., Jones,
549 P., Rasmusson, E., Roeckner, E., Ropelewski, C., Santer, B., et al., 1999.
550 Detection and attribution of recent climate change: A status report. Bul-
551 letin of the American Meteorological Society 80 (12), 26312660.

552 Barnett, T., Santer, B., Jones, P., Bradley, R., Briffa, K., Jan. 1996. Esti-
553 mates of low frequency natural variability in near-surface air temperature.
554 The Holocene 6 (3), 255–263.

555 Bendle, J., Rosell-Mele, A., 2007. High-resolution alkenone sea surface tem-
556 perature variability on the North Icelandic Shelf: implications for Nordic
557 Seas palaeoclimatic development during the Holocene. The Holocene
558 17 (1), 9.

559 Berger, W., Heath, G., 1968. Vertical mixing in pelagic sediments. J. mar.
560 Res 26 (2), 134143.

561 Boudreau, B., 1998. Mean mixed depth of sediments: The wherefore and the
562 why. Limnology and Oceanography, 524526.

563 Brassell, S. C., Eglinton, G., Marlowe, I. T., Pflaumann, U., Sarnthein, M.,
564 Mar. 1986. Molecular stratigraphy: a new tool for climatic assessment.
565 Nature 320 (6058), 129.

566 Cacho, I., Grimalt, J. O., Canals, M., Sbaifi, L., Shackleton, N. J., Schoen-
567 feld, J., Zahn, R., 2001. Variability of the western Mediterranean Sea sur-
568 face temperature during the last 25,000 years and its connection with the
569 Northern Hemisphere climatic changes. Paleoceanography 16 (1), PP. 40–
570 52.

571 Calvo, E., Grimalt, J., Jansen, E., Jul. 2002. High resolution U37K sea sur-
572 face temperature reconstruction in the Norwegian Sea during the Holocene.
573 Quaternary Science Reviews 21 (1213), 1385–1394.

574 Cleroux, C., Debret, M., Cortijo, E., Duplessy, J., Dewilde, F., Reijmer, J.,
575 Massei, N., Feb. 2012. High-resolution sea surface reconstructions off Cape
576 Hatteras over the last 10ka. Paleoclimatology 27, 14 PP.

577 De Vernal, A., Rosell-Mel, A., Kucera, M., Hillaire-Marcel, C., Eynaud, F.,
578 Weinelt, M., Dokken, T., Kageyama, M., 2006. Comparing proxies for
579 the reconstruction of LGM sea-surface conditions in the northern north
580 atlantic. Quaternary Science Reviews 25 (21-22), 28202834.

581 Dekens, P., Lea, D. W., Pak, D. K., Spero, H. J., 2001. Core top calibration
582 of Mg/Ca in tropical foraminifera: refining paleo-temperature estimation.
583 University of California, Santa Barbara.

584 Ditlevsen, P. D., Svensmark, H., Johnsen, S., 1996. Contrasting atmospheric
585 and climate dynamics of the last-glacial and Holocene periods. Nature
586 379 (6568), 810–812.

587 Dooe-Rolinski, H., Rogalla, U., Scheeder, G., Lueckge, A., Rad, U. v., Aug.
588 2001. High-resolution temperature and evaporation changes during the
589 Late Holocene in the northeastern Arabian Sea. Paleoclimatology 16 (4),
590 P. 358.

591 Emeis, K., Struck, U., Blanz, T., Kohly, A., Vo, M., Apr. 2003. Salinity
592 changes in the central Baltic Sea (NW Europe) over the last 10000 years.
593 The Holocene 13 (3), 411 –421.

- 594 Farmer, E. J., Chapman, M. R., Andrews, J. E., Dec. 2008. Centennial-
595 scale Holocene North Atlantic surface temperatures from Mg/Ca ratios in
596 *Globigerina bulloides*. *Geochemistry Geophysics Geosystems* 9.
- 597 Fraile, I., Schulz, M., Mulitza, S., Kucera, M., 2008. Predicting the global
598 distribution of planktonic foraminifera using a dynamic ecosystem model.
599 *Biogeosciences* 5 (3), 891911.
- 600 Gong, C., Hollander, D. J., Feb. 1999. Evidence for differential degradation of
601 alkenones under contrasting bottom water oxygen conditions: implication
602 for paleotemperature reconstruction. *Geochimica et Cosmochimica Acta*
603 63 (3-4), 405–411.
- 604 Guinasso, N. L. G., Schink, D. R., 1975. Quantitative Estimates of Biologi-
605 cal Mixing Rates in Abyssal Sediments. *Journal of Geophysical Research*
606 80 (21), PP. 3032–3043.
- 607 Harada, N., Ahagon, N., Sakamoto, T., Uchida, M., Ikehara, M., Shibata, Y.,
608 Aug. 2006. Rapid fluctuation of alkenone temperature in the southwestern
609 Okhotsk Sea during the past 120 ky. *Global and Planetary Change* 53 (1-
610 2), 29–46.
- 611 Hasselmann, K., Dec. 1976. Stochastic climate models Part I. Theory. *Tellus*
612 28 (6), 473–485.
- 613 Hoefs, M. J. L., Versteegh, G. J. M., Rijpstra, W. I. C., Leeuw, J. W. d.,
614 Damst, J. S. S., 1998. Postdepositional oxic degradation of alkenones: Im-
615 plications for the measurement of palaeo sea surface temperatures. *Paleo-*
616 *ceanography* 13 (1), 42–49.

617 Huybers, P., Curry, W., May 2006. Links between annual, Milankovitch and
618 continuum temperature variability. *Nature* 441 (7091), 329–332.

619 Huybers, P., Wunsch, C., 2003. Rectification and precession signals in the
620 climate system. *Geophysical Research Letters* 30 (19), n/an/a.

621 Isono, D., Yamamoto, M., Irino, T., Oba, T., Murayama, M., Nakamura, T.,
622 Kawahata, H., Jul. 2009. The 1500-year climate oscillation in the midlati-
623 tude North Pacific during the Holocene. *Geology* 37 (7), 591–594.

624 Jungclauss, J. H., Lorenz, S. J., Timmreck, C., Reick, C. H., Brovkin, V.,
625 Six, K., Segschneider, J., Giorgetta, M. A., Crowley, T. J., Pongratz, J.,
626 Krivova, N. A., Vieira, L. E., Solanki, S. K., Klocke, D., Botzet, M.,
627 Esch, M., Gayler, V., Haak, H., Raddatz, T. J., Roeckner, E., Schnur,
628 R., Widmann, H., Claussen, M., Stevens, B., Marotzke, J., 2010. Climate
629 and carbon-cycle variability over the last millennium. *Clim. Past* 6 (5),
630 723–737.

631 Kennedy, J., Rayner, N., Smith, R., Saunby, M., Parker, D., 2011a. Reassess-
632 ing biases and other uncertainties in sea-surface temperature observations
633 measured in situ since 1850, part 2: biases and homogenisation. *JGR At-*
634 *mospheres*.

635 Kennedy, J. J., Rayner, N. A., Smith, R. O., Parker, D. E., Saunby, M.,
636 Jul. 2011b. Reassessing biases and other uncertainties in sea surface tem-
637 perature observations measured in situ since 1850: 1. Measurement and
638 sampling uncertainties. *Journal of Geophysical Research* 116, 13 PP.

639 Kim, J., Meggers, H., Rimbu, N., Lohmann, G., Freudenthal, T., Mller, P. J.,
640 Schneider, R. R., May 2007. Impacts of the North Atlantic gyre circulation
641 on Holocene climate off northwest Africa. *Geology* 35 (5), 387–390.

642 Kim, J., Rimbu, N., Lorenz, S. J., Lohmann, G., Nam, S., Schouten, S.,
643 Rhlemann, C., Schneider, R. R., Nov. 2004. North Pacific and North At-
644 lantic sea-surface temperature variability during the Holocene. *Quaternary*
645 *Science Reviews* 23 (20-22), 2141–2154.

646 Kirchner, J., Jun. 2005. Aliasing in $1/f^\alpha$ noise spectra: Origins, conse-
647 quences, and remedies. *Physical Review E* 71 (6).

648 Laepple, T., Werner, M., Lohmann, G., 2011. Synchronicity of Antarc-
649 tic temperatures and local solar insolation on orbital timescales. *Nature*
650 471 (7336), 91–94.

651 Lamy, F., Rhlemann, C., Hebbeln, D., Wefer, G., Jun. 2002. High- and low-
652 latitude climate control on the position of the southern Peru-Chile Current
653 during the Holocene. *Paleoceanography* 17, 10 PP.

654 Lea, D. W., Mashiotta, T. A., Spero, H. J., Aug. 1999. Controls on magne-
655 sium and strontium uptake in planktonic foraminifera determined by live
656 culturing. *Geochimica et Cosmochimica Acta* 63 (16), 2369–2379.

657 Leduc, G., Schneider, R., Kim, J. H., Lohmann, G., 2010. Holocene and
658 Eemian sea surface temperature trends as revealed by alkenone and Mg/Ca
659 paleothermometry. *Quaternary Science Reviews* 29 (7-8), 9891004.

660 Lohmann, G., Pfeiffer, M., Laepple, T., Leduc, G., Kim, J. H., 2012. A

661 model-data comparison of the Holocene global sea surface temperature
662 evolution. *Climate of the Past Discussions* 8, 10051056.

663 Lomb, N. R., Feb. 1976. Least-squares frequency analysis of unequally spaced
664 data. *Astrophysics and Space Science* 39 (2), 447–462.

665 Lueckge, A., Mohtadi, M., Rhlemann, C., Scheeder, G., Vink, A., Reinhardt,
666 L., Wiedicke, M., Feb. 2009. Monsoon versus ocean circulation controls
667 on paleoenvironmental conditions off southern Sumatra during the past
668 300,000 years. *Paleoceanography* 24, 14 PP.

669 Marchitto, T. M., Muscheler, R., Ortiz, J. D., Carriquiry, J. D., van Geen,
670 A., Dec. 2010. Dynamical Response of the Tropical Pacific Ocean to Solar
671 Forcing During the Early Holocene. *Science* 330 (6009), 1378–1381.

672 Mashiotto, T. A., Lea, D. W., Spero, H. J., 1999. Glacialinterglacial changes
673 in subantarctic sea surface temperature and $\delta^{18}\text{O}$ -
674 water using foraminiferal Mg . *Earth and Planetary Science Letters* 170 (4),
675 417432.

676 Mix, A. C., Jun. 2006. Running hot and cold in the eastern equatorial pacific.
677 *Quaternary Science Reviews* 25 (1112), 1147–1149.

678 Mueller, P. J., Kirst, G., Ruhland, G., Von Storch, I., Rosell-Mel, A., 1998.
679 Calibration of the alkenone paleotemperature index U_{37K}’based on core-
680 tops from the eastern South Atlantic and the global ocean (60 N-60 S).
681 *Geochimica et Cosmochimica Acta* 62 (10), 17571772.

682 Ohkouchi, N., Eglinton, T. I., Keigwin, L. D., Hayes, J. M., Nov. 2002.

683 Spatial and Temporal Offsets Between Proxy Records in a Sediment Drift.
684 Science 298 (5596), 1224 –1227.

685 Pelletier, J. D., 1998. The power spectral density of atmospheric temperature
686 from time scales of 10-2 to 106 yr. Earth and Planetary Science Letters
687 158 (3-4), 157164.

688 Percival, D. B., Walden, A. T., 1993. Spectral analysis for physical applica-
689 tions: multitaper and conventional univariate techniques. Cambridge Univ
690 Pr.

691 Rayner, N., Brohan, P., Parker, D., Folland, C., Kennedy, J., Vanicek, M.,
692 Ansell, T., Tett, S., 2006. Improved analyses of changes and uncertain-
693 ties in sea surface temperature measured in situ since the mid-nineteenth
694 century: the HadSST2 dataset. Journal of Climate 19 (3), 446469.

695 Regenberg, M., Nrnberg, D., Steph, S., Groeneveld, J., Garbe-Schnberg, D.,
696 Tiedemann, R., Dullo, W.-C., Jul. 2006. Assessing the effect of dissolution
697 on planktonic foraminiferal Mg/Ca ratios: Evidence from caribbean core
698 tops. Geochemistry Geophysics Geosystems 7, 23 PP.

699 Rhines, A., Huybers, P., 2011. Estimation of spectral power laws in time
700 uncertain series of data with application to the Greenland Ice Sheet Project
701 2 d18O record. Journal of Geophysical Research 116 (D1), D01103.

702 Richey, J., Hollander, D., Flower, B., Eglinton, T., 2011. Merging late
703 holocene molecular organic and foraminiferal-based geochemical records
704 of sea surface temperature in the gulf of mexico. Paleoceanography 26 (1),
705 PA1209.

706 Rodrigues, T., Grimalt, J. O., Abrantes, F. G., Flores, J. A., Lebreiro, S. M.,
707 Jul. 2009. Holocene interdependences of changes in sea surface tempera-
708 ture, productivity, and fluvial inputs in the Iberian continental shelf (Tagus
709 mud patch). *Geochemistry Geophysics Geosystems* 10 (7).

710 Sachs, J., 2007. Cooling of Northwest Atlantic slope waters during the
711 Holocene. *Geophysical research letters* 34 (3), L03609.

712 Sadekov, A., Eggins, S. M., Deckker, P. D., Kroon, D., Mar. 2008. Uncertain-
713 ties in seawater thermometry deriving from intratest and intertest Mg/Ca
714 variability in globigerinoides ruber. *Paleoceanography* 23, 12 PP.

715 Schiffelbein, P., Hills, S., 1984. Direct assessment of stable isotope variability
716 in planktonic foraminifera populations. *Palaeogeography, palaeoclimatol-
717 ogy, palaeoecology* 48 (2-4), 197213.

718 Schneider, B., Leduc, G., Park, W., 2010. Disentangling seasonal signals in
719 holocene climate trends by satellite-model-proxy integration. *Paleoceanog-
720 raphy* 25 (4), PA4217.

721 Shackleton, N. J., Imbrie, J., 1990. The d18O spectrum of oceanic deep water
722 over a five-decade band. *Climatic change* 16 (2), 217230.

723 Sonzogni, C., Bard, E., Rostek, F., Dollfus, D., Rosell-Mel, A., Eglinton, G.,
724 May 1997. Temperature and salinity effects on alkenone ratios measured
725 in surface sediments from the indian ocean. *Quaternary Research* 47 (3),
726 344–355.

727 Steinke, S., Kienast, M., Groeneveld, J., Lin, L. C., Chen, M. T., Rendle-
728 Bhring, R., 2008. Proxy dependence of the temporal pattern of deglacial

729 warming in the tropical south china sea: toward resolving seasonality.
730 Quaternary Science Reviews 27 (7), 688700.

731 Stott, L., Cannariato, K., Thunell, R., Haug, G. H., Koutavas, A., Lund, S.,
732 2004. Decline of surface temperature and salinity in the western tropical
733 Pacific Ocean in the Holocene epoch. Nature 431 (7004), 56–59.

734 Wallace, J. M., Smith, C., Jiang, Q., Sep. 1990. Spatial patterns of
735 atmosphere-ocean interaction in the northern winter. Journal of Climate
736 3 (9), 990–998.

737 Weldeab, S., Lea, D. W., Schneider, R. R., Andersen, N., Jun. 2007. 155,000
738 Years of West African Monsoon and Ocean Thermal Evolution. Science
739 316 (5829), 1303–1307.

740 Wunsch, C., 2009. A perpetually running enso in the pliocene? Journal of
741 Climate 22 (12), 3506–3510.

742 Xu, J., Holbourn, A., Kuhnt, W., Jian, Z., Kawamura, H., Aug. 2008.
743 Changes in the thermocline structure of the Indonesian outflow during
744 Terminations I and II. Earth and Planetary Science Letters 273 (1-2),
745 152–162.

746 Zhao, M., Huang, C., Wang, C., Wei, G., Jun. 2006. A millennial-scale U37K
747 sea-surface temperature record from the South China Sea (8N) over the
748 last 150 kyr: Monsoon and sea-level influence. Palaeogeography, Palaeo-
749 climatology, Palaeoecology 236 (12), 39–55.

Table 1: Proxy data used in the main study

Nr.	Name	Ref.	Lat.	Lon.	sed. rate	mean Δt (yr)	interp. Δt (yr)	duration	proxy	seasonal range
1	MD03-2707	(Woldeab et al., 2007)	2.5	9.4	55	36	100	6600	Mg/Ca G.ruber (pink)	3.4
2	MD98-2176	(Stott et al., 2004)	-5.0	133.4	50	43	100	6818	Mg/Ca G.ruber (white)	3.3
3	MD99-2155	(Farmer et al., 2008)	57.4	-27.9	166	52	100	6440	Mg/Ca G.bulloides	4.2
4	MD99-2203	(Cleroux et al., 2012)	35.0	-75.2	53	19	100	6374	Mg/Ca G.ruber (white)	7.4
5	MD98-2181	(Stott et al., 2004)	6.3	125.8	80	43	150	6969	Mg/Ca G.ruber (white)	1.7
6	MV99-GC41/PC14	(Marchitto et al., 2010)	25.2	247.3	79	90	150	6091	Mg/Ca G.bulloides	7.5
1	SO90-39KG/56KA	(Dooze-Rolinski et al., 2001)	24.8	65.9	123	20	100	4880	Uk37	5.4
2	GeoB6007	(Kim et al., 2007)	30.9	-10.3	65	31	100	6750	Uk37	5.2
3	MD97-2151	(Zhao et al., 2006)	8.7	109.9	39	49	100	6020	Uk37	3.9
4	SSDP-102	(Kim et al., 2004)	35.0	128.9	216	61	150	6870	Uk37	12.8
5	IOW 225514	(Emeis et al., 2003)	57.8	8.7	66	72	150	5980	Uk37	11.7
6	CH07-98-GGC19	(Sachs, 2007)	36.9	-74.6	27	68	150	6470	Uk37	12.2
7	OCE326-GGC30	(Sachs, 2007)	43.9	-62.8	30	72	150	6940	Uk37	13.7
8	KR02-06	(Isono et al., 2009)	36.0	141.8	30	51	150	7013	Uk37	12.6
9	MD952011	(Calvo et al., 2002)	67.0	7.6	74	58	200	6450	Uk37	5.3
10	MD01-2412	(Harada et al., 2006)	44.5	145.0	95	73	200	6920	Uk37	14.1
11	D13882	(Rodrigues et al., 2009)	38.6	-9.5	55	53	200	6530	Uk37	5.6
12	IOW 225517	(Emeis et al., 2003)	57.7	7.1	52	94	200	5170	Uk37	11.7
13	JR51-GC35	(Bendle and Rosell-Mele, 2007)	67.0	-18.0	48	98	200	6880	Uk37	4.6
14	GeoB 3313-1	(Lamy et al., 2002)	-41.0	-74.5	107	90	200	6930	Uk37	4.3
15	GeoB 5901-2	(Kim et al., 2007)	36.4	-7.1	13	80	200	5840	Uk37	5.6
16	SO139-74KL	(Lueckge et al., 2009)	-6.5	103.8	106	78	200	5870	Uk37	1.7

Listed are the core number, core name, reference, latitude in $^{\circ}$ N, longitude in $^{\circ}$ E, sedimentation rates in cm/ky, the mean sampling interval in yr, the interpolated resolution in years, the duration of the record in years, and the seasonal range of the modern SST in $^{\circ}$ C. Values regarding the proxy records are computed over the last 7 ky BP, where BP is with respect to 1950 AD.

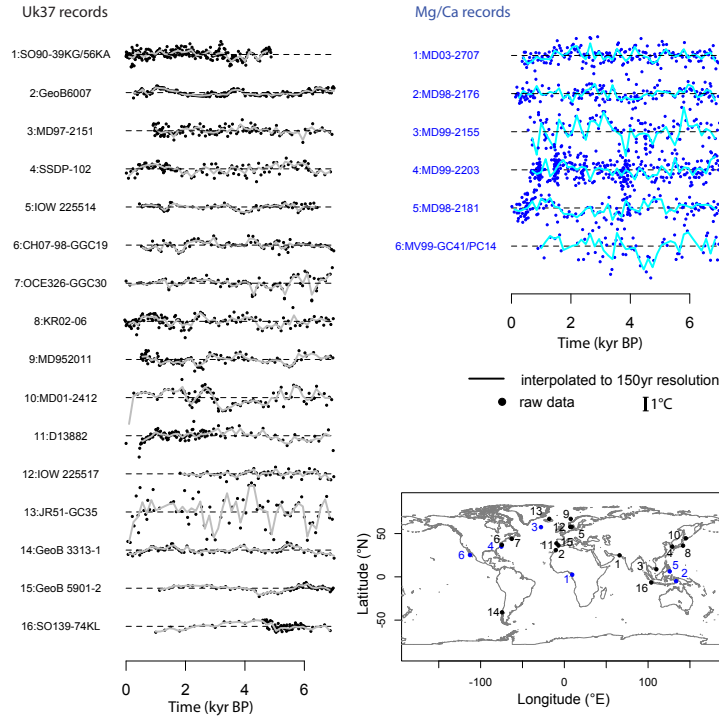


Figure 1: Map of proxy locations and proxy time series of Uk37 (black) and Mg/Ca (blue). All records are linearly detrended. The original data (dots), and the data interpolated to a common 150 year resolution (lines) are shown to facilitate visual intercomparison. The common y-axis scale for all records is show in the legend.

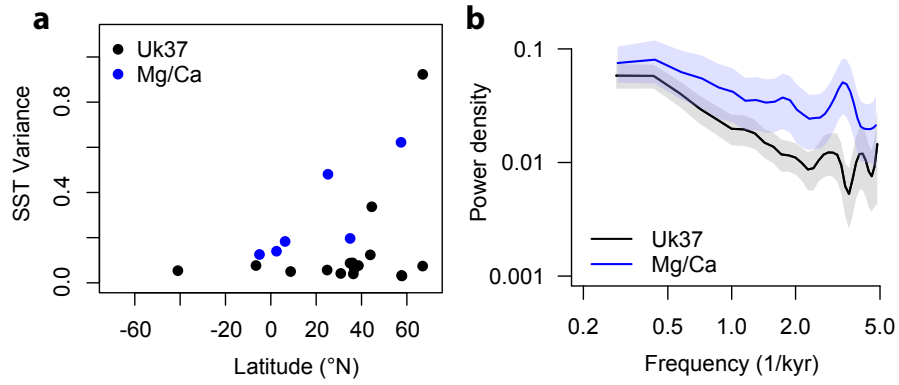


Figure 2: Spatial and spectral comparison of Mg/Ca and Uk37 derived SST variability **(a)** Variance of the proxy time series against latitude for Uk37 and Mg/Ca. All time series were interpolated to 150 yr prior to the variance calculation to minimize influences of the sampling interval on the variance estimate. **(b)** Spectral estimates of Uk37 and Mg/Ca SST records. The mean of the spectral estimates of the globally distributed single records is shown. 95% confidence intervals are indicated by shading

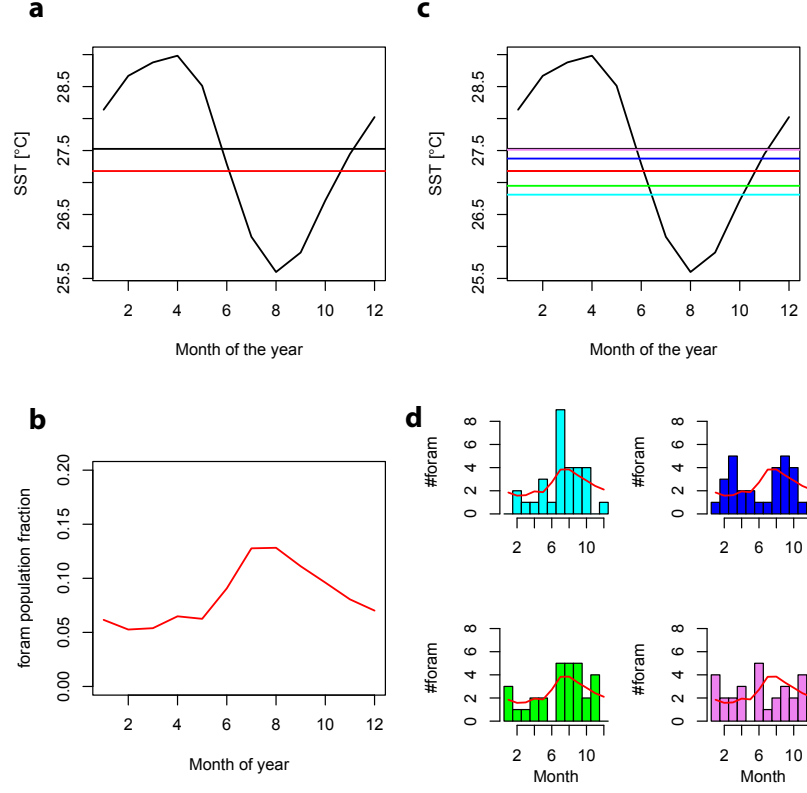


Figure 3: Example of aliasing of the seasonal cycle for the Mg/Ca record from core MD03-2707 (Weldeab et al., 2007). **(a)** The climatological seasonal cycle of sea surface temperature (SST) at the core site from instrumental records (black) and the annual mean SST (horizontal black line). **(b)** The seasonal cycle of *G. ruber* population at the core site from the PLAFOM model (Fraile et al., 2008). Weighting SST seasonality by population seasonality gives a bias toward cooler temperature (red horizontal line in **(a)**). **(c,d)** Because a typical Mg/Ca sample only consists of 30 foraminifera tests, the sampled seasonal cycle has a substantial stochastic component, indicated by the histograms in **(d)**, that leads to variations in recorded temperature that are indicated by the correspondingly colored horizontal lines in **(c)**.

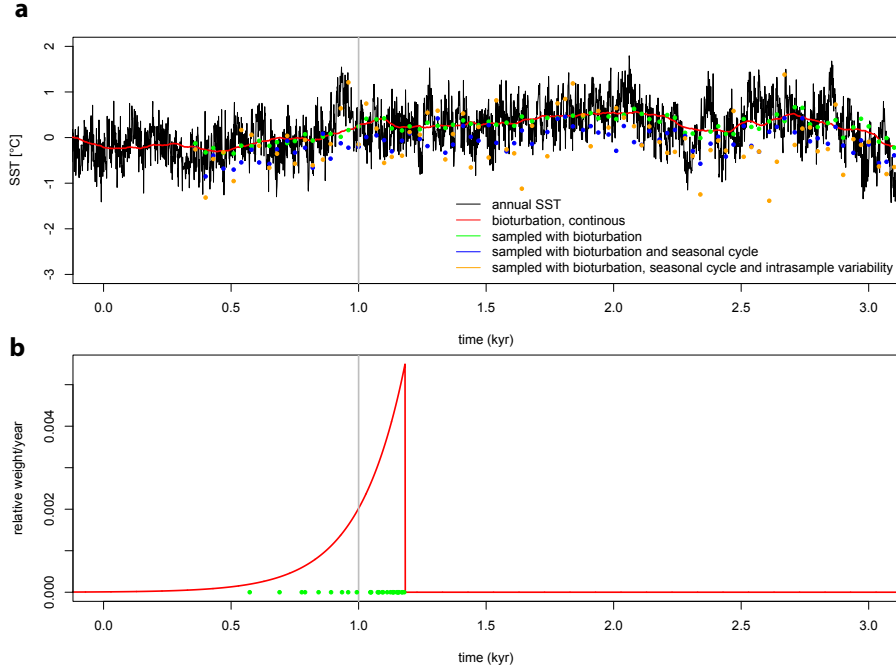


Figure 4: Example of bioturbation and aliasing at core MD03-2707 (Woldeab et al., 2007). **(a)** A synthetic SST time series appropriate for this core site (black) is sampled in various manners and subject to bioturbation. **(b)** The impulse response to bioturbation at this core site (red line) for a sample at 1 kyr (vertical grey line), assuming $\delta = 10\text{cm}$. In the case of continuous sampling, bioturbation leads to a smoothed and lagged version of the SST record (red line in (a)). However, the Mg/Ca measurements consist of a limited number of foraminiferal tests (green dots in (b)), leading to additional variability in the sampled record (green dots in (a)) caused by aliasing of the interannual variability. In addition, aliasing of the seasonal cycle leads to further variability and an offset in the mean (blue dots in (a), c.f. Fig. 3). Finally, intratest and measurement noise contribute additional noise that is estimated to have a standard deviation of 0.5°C for this record (orange dots in (a)).

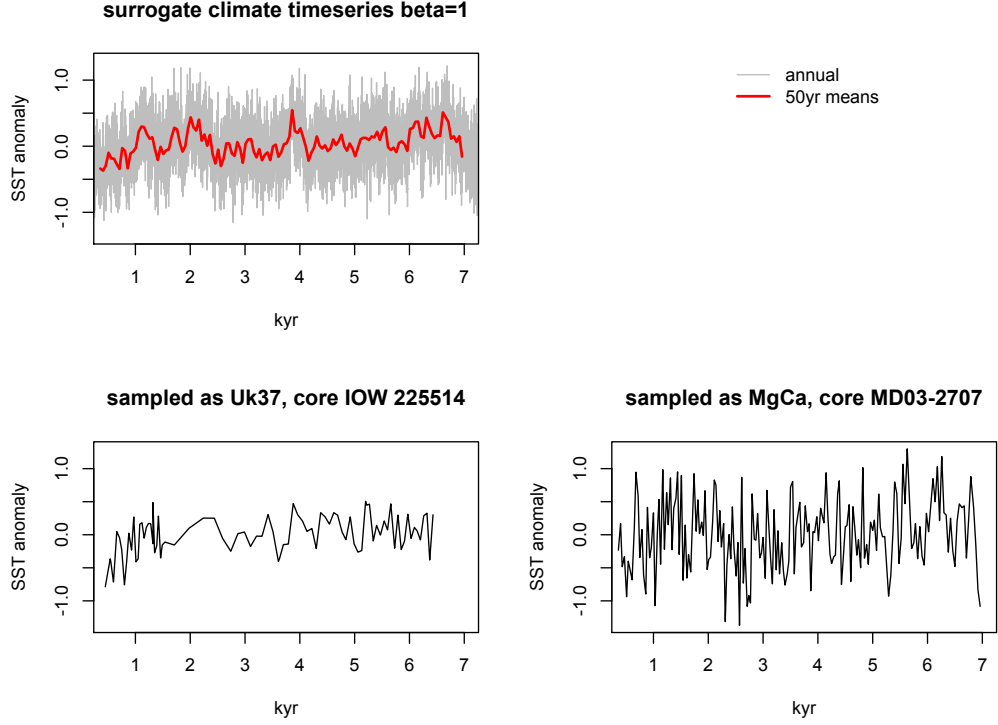


Figure 5: An example of corrupting a synthetic temperature time series according to the noise and sampling regime found in Mg/Ca and Uk37 records. Top left: A realization of a temperature time series simulated using $\beta = 1$. Lower panels: sampling according to the biophysical model for Uk37 (left) and Mg/Ca (right) gives very different proxy time series behavior. The Uk37 record has slightly suppressed variability because of the effects of bioturbation, whereas the Mg/Ca record has greater variability because of aliasing of the seasonal cycle.

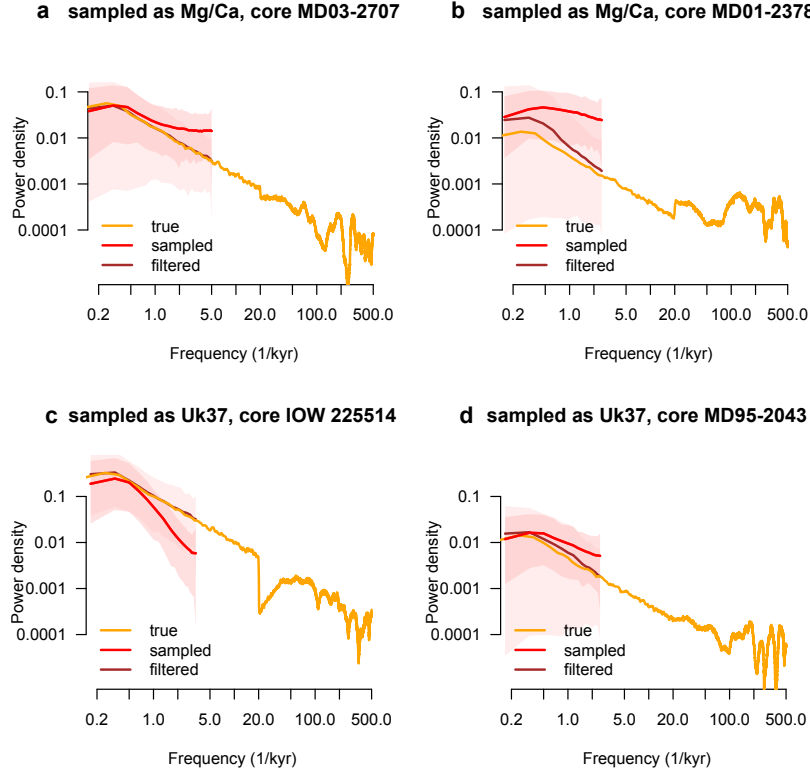


Figure 6: Demonstration of the correction process for synthetic Mg/Ca and Uk37 records. Top row: for Mg/Ca records having sampling resolutions of 36 years (a, MD03-2707 (Weldeab et al., 2007)) and 125 years (b, MD01-2378 (Xu et al., 2008)). Spectra estimated from random time series having $\beta = 1$ (orange), corrupted using a 10cm bioturbation width and a noise contribution, η of 0.45°C (red). Corruption of the spectral estimate is greatest at high frequencies because unresolved variability is preferentially aliased to these frequencies and because the relatively smaller amount of background variability is more easily disrupted in a fractional sense. After filtering, the original spectrum is recovered in expectation (red), though the 95% confidence interval is increased (shading) owing to uncertainties associated with the correction process. Note that confidence intervals are centered on their respective estimates and are darker where they overlap. Lower row: For Uk37 records having sampling resolutions of 72 years (c, IOW 225514 (Emeis et al., 2003)) and 130 years (d, MD95-2043 (Cacho et al., 2001)). Time series are simulated using an error term, η of 0.25°C . The corrupted spectra shows less variability at high frequencies because the influence of bioturbation is greater than that of measurement noise and because there is no aliasing. The low-resolution result remains less reliable than the high-resolution one, though the discrepancy is less marked than for the Mg/Ca records.

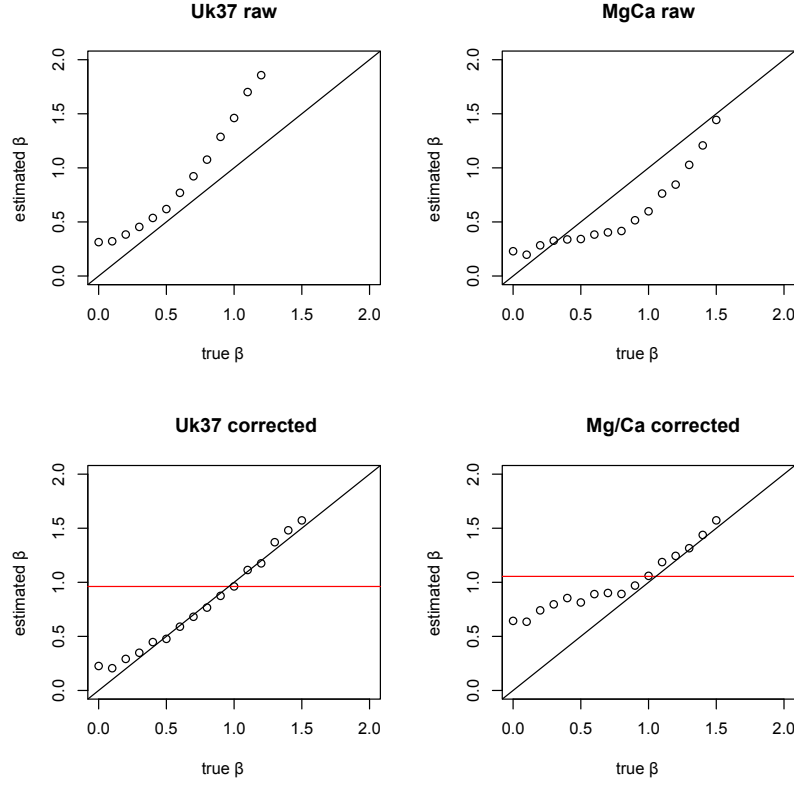


Figure 7: Test of the correction algorithm’s ability to recover power-law slopes. Random time series following the spectral model of Eq. 2 with $\beta = \{0, 0.1, \dots, 1.9, 1.5\}$ are simulated using a 10cm bioturbation width, standard deviations of η of 0.25°C and 0.45°C for Uk37 and Mg/Ca, respectively, and individual core parameters for sampling intervals. β is estimated both directly (top row) and after application of the spectral correction algorithm (lower row). For Uk37, the sampling and bioturbation generally leads to an increase in the estimated β when no correction is applied, whereas for Mg/Ca the higher noise level and aliasing leads to a smaller β . The correction filter yields good estimates when the true β is greater than 0.1 for Uk37 and 0.7 for Mg/Ca records, but for shallower power-laws there is a positive bias. The bias results from difficulties in separating signal from noise when both are close to white and because β is constrained to always be positive. Importantly, the method appears unbiased in the range of the reconstructed β from the observations (horizontal red lines).

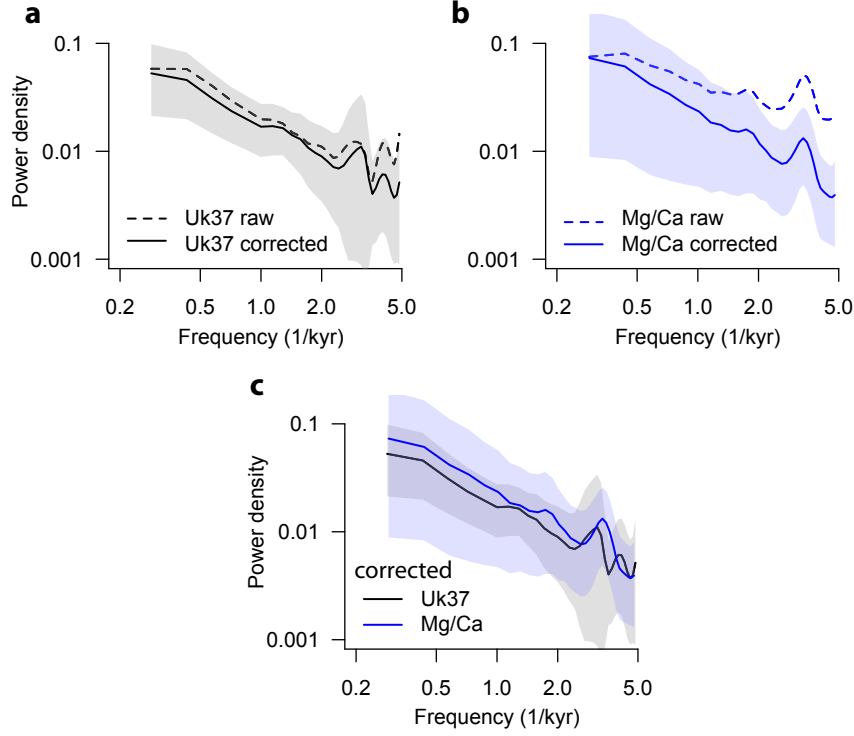


Figure 8: Spectral estimates of the proxy derived SST, raw and after correcting for sampling and noise. (a) for Uk37, (b) for Mg/Ca, (c) comparison of the corrected Uk37 and Mg/Ca spectra. After correction, both spectral estimates are consistent. 95% confidence intervals, indicated by shading, account for the correction process of Uk37 and Mg/Ca where appropriate.

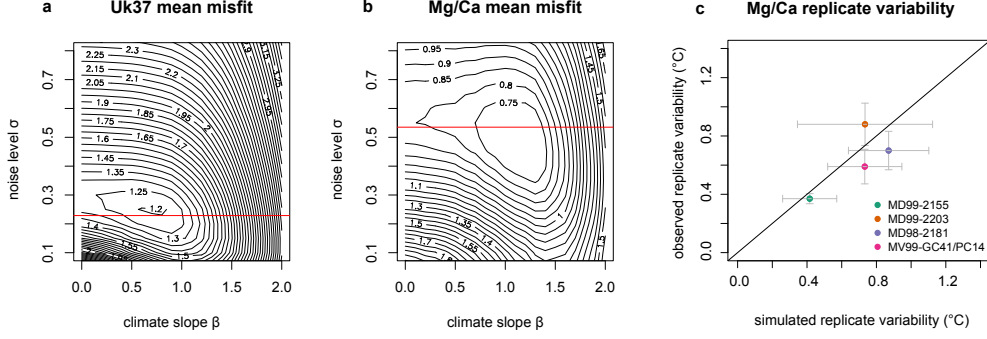


Figure 9: Misfit between observed and modeled spectra for Uk37 **(a)** and Mg/Ca **(b)** as a function of β and the standard deviation of η . The mean misfit of all cores is shown and indicates distinct minima for both classes of records. Horizontal red lines indicate values of independently reported measurement error for Uk37 from the GHOST database (Leduc et al., 2010) and the mean observed measurement and intrasample error for Mg/Ca. The latter was estimated from the observed replicate error subtracting the contribution from seasonal aliasing indicated by the correction algorithm. **(c)** Comparison of simulated and observed replicate variability of Mg/Ca records. Error bars represent 2 standard deviations. Error bars of the simulated replicate variability are inferred from Monte Carlo experiments using synthetic records designed according to the characteristics of each record. For MD98-2181, the reported replicate standard deviation from Stott et al. (2004) is shown, whereas the other three replicater errors are calculated from data provided through personal communication.